Crystal Structures of Human Glutaryl-CoA Dehydrogenase with and without an Alternate Substrate: Structural Bases of Dehydrogenation and Decarboxylation Reactions†,‡

Zhuji Fu,§,|| Ming Wang,§,|| Rosemary Paschke,§ K. Sudhindra Rao,⊥ Frank E. Frerman,⊥ and Jung-Ja P. Kim*,§

Department of Biochemistry, Medical College of Wisconsin, Milwaukee, Wisconsin 53226, and Departments of Pediatrics and Pharmaceutical Sciences, The University of Colorado Health Sciences Center, Denver, Colorado 80262

Received April 8, 2004; Revised Manuscript Received May 26, 2004

ABSTRACT: Acyl-CoA dehydrogenases (ACDs) are a family of flavoenzymes that metabolize fatty acids and some amino acids. Of nine known ACDs, glutaryl-CoA dehydrogenase (GCD) is unique: in addition to the α,β-dehydrogenation reaction, common to all ACDs, GCD catalyzes decarboxylation of glutaryl-CoA to produce CO_2 and crotonyl-CoA. Crystal structures of GCD and its complex with 4-nitrobutyryl-CoA have been determined to 2.1 and 2.6 Å, respectively. The overall polypeptide folds are the same and similar to the structures of other family members. The active site of the unliganded structure is filled with water molecules that are displaced when enzyme binds the substrate. The structure strongly suggests that the mechanism of dehydrogenation is the same as in other ACDs. The substrate binds at the *re* side of the FAD ring. Glu370 abstracts the C2 *pro-R* proton, which is acidified by the polarization of the thiolester carbonyl oxygen through hydrogen bonding to the 2′-OH of FAD and the amide nitrogen of Glu370. The C3 *pro-R* proton is transferred to the N(5) atom of FAD. The structures indicate a plausible mechanism for the decarboxylation reaction. The carbonyl polarization initiates decarboxylation, and Arg94 stabilizes the transient crotonyl-CoA anion. Protonation of the crotonyl-CoA anion occurs by a 1,3-prototropic shift catalyzed by the conjugated acid of the general base, Glu370. A tight hydrogen-bonding network involving γ-carboxylate of the enzyme-bound glutaconyl-CoA, with Tyr369, Glu87, Arg94, Ser95, and Thr170, optimizes orientation of the γ-carboxylate for decarboxylation. Some pathogenic mutations are explained by the structure. The mutations affect protein folding, stability, and/or substrate binding, resulting in inefficient/inactive enzyme.

Glutaryl-CoA dehydrogenase (GCD)[1] is a member of the acyl-CoA dehydrogenase (ACD) family of flavoproteins that catalyzes the oxidation of acyl-CoA thioesters to the corresponding 2-enoyl-CoA products. There are nine known members in the ACD family, five of which are involved in fatty acid oxidation and four, including GCD, involved in amino acid oxidation. The physiological oxidant of GCD is electron transfer flavoprotein, the common electron acceptor of all nine ACDs (*1*, *2*). There is considerable identity among the primary sequences of the ACDs, and the overall folding of the polypeptides of these dehydrogenases is highly conserved in the four cases in which the three-dimensional structures have been determined (*3*−*7*). The catalytic mechanisms of these enzymes have common features (*8*). The position of the catalytic base, a glutamate residue that initiates the catalytic cycle, is located in the same relative position in seven of the nine mammalian ACDs (*9*−*11*). In the remaining two dehydrogenases, long-chain acyl-CoA dehydrogenase (LCAD) and isovaleryl-CoA dehydrogenase (IVD), the glutamate catalytic base is located on a different helix, topologically conserved, but situated over 100 residues away from the conserved glutamate of other seven ACDs in the primary sequence (*5*, *12*).

GCD is unique among the ACD family members, owing to its additional catalytic function of decarboxylation. The enzyme catalyzes the oxidative decarboxylation of the γ-carboxylate of the substrate, glutaryl-CoA, to yield crotonyl-CoA and CO_2. Although the mechanism of dehydrogenation appears similar to that of other ACDs (*13*−*17*), there are significant differences in the reaction catalyzed by GCD, suggesting that there are likely to be structural differences in the active site of this dehydrogenase. First, the substrate has a carboxylate group bound to C4 making GCD the only ACD that catalyzes the oxidation of a substrate containing an anionic functional group in the acyl moiety. This is an important factor when considering the number of anionic species that participate in the proposed catalytic pathway (*13*, *17*). These anions include an anionic dehydrogenase flavin

† This research is supported by NIH Grants GM29076 (J.-J.P.K) and NS 39339 (F.E.F.).

‡ The atomic coordinates and structure factors have been deposited in the Protein Data Bank (PDB codes 1SIQ for the uncomplexed and 1SIR for the substrate-bound structures).

* Corresponding author. Phone: (414) 456-8479. Fax: (414) 456-6510. E-mail: jjkim@mcw.edu.

§ Medical College of Wisconsin.

|| Contributed equally to this work.

⊥ The University of Colorado Health Sciences Center.

[1] Abbreviations: ACD, acyl-CoA dehydrogenase; GCD, glutaryl-CoA dehydrogenase; IVD, isovaleryl-CoA dehydrogenase; MCAD, medium-chain acyl-CoA dehydrogenase; SCAD, short-chain acyl-CoA dehydrogenase; IBD, isobutyryl-CoA dehydrogenase; 4-NB-CoA, 4-nitrobutyryl-CoA or 4-nitrobut-2-enoyl-CoA.

10.1021/bi049290c CCC: $27.50
Published on Web 07/07/2004

semiquinone and an anionic dehydrogenase flavin hydroquinone (*16*). In addition, Westover and co-workers have presented evidence for a crotonyl-CoA anion following decarboxylation of glutaconyl-CoA, the reaction intermediate (*17*). This necessitates the protonation of the C4 anion of crotonyl-CoA. In the case of a bacterial GCD, the conjugate acid of the base that initiates catalysis apparently donates this proton in a 1,3-prototropic shift (*13*). Arg94 has been considered both as a hydrogen bond donor to the γ-carboxylate of glutaryl-CoA and as an electrostatic catalyst that stabilizes negative charge during catalysis (*18*). The decarboxylation reaction is not obligatorily linked to oxidation because there are a number of alternate substrates for GCD. Among these alternate substrates, 4-nitrobutyryl-CoA is isostructural and isoelectronic with glutaryl-CoA; its k_{cat} value is 2% that of glutaryl-CoA, and the K_m of GCD for 4-nitrobutyryl-CoA is only 3.8-fold greater than the K_m for glutaryl-CoA (*19*).

Here, we report the three-dimensional structures of human GCD in its uncomplexed form and in complex with 4-nitrobutyryl-CoA. A preliminary structure of uncomplexed GCD was reported earlier (*20*). The structure confirms Glu370 as the catalytic base and identifies residues that form the active site cavity. We have compared the GCD structure to those of four other ACDs that have been determined. Similarities and differences between GCD and these other dehydrogenase structures allow us to propose the structural bases for the mechanisms of the dehydrogenation and decarboxylation reactions.

MATERIALS AND METHODS

N-[2-Hydroxyethyl]piperazine-*N*′-[2-ethanesulfonic acid] (HEPES), 2-[*N*-morpholino]ethanesulfonic acid (MES), and acetoacetyl-CoA were purchased from Sigma. Octyl β-D-glucopyranoside was purchased from Calbiochem, and poly(ethylene glycol)monomethyl ether 5000 was from Aldrich. 4-Nitrobutyryl-CoA was synthesized as described previously (*19*).

Enzyme Purification and Crystallization. Human GCD was overexpressed in *Escherichia coli* and purified as previously described *(16)*. The purified GCD was dialyzed against 20 mM HEPES, pH 7.0 containing 100 mM NaCl, concentrated to a final concentration of approximately 15 mg/mL, and stored at −80 °C until needed. Crystals were obtained by vapor diffusion using the hanging drop technique (*21*) by mixing equal volumes of GCD solution (15 mg/mL in 20 mM HEPES buffer, pH 7.5) with precipitating solution (100 mM MES, pH 6.5 containing 30% poly(ethyleneglycol)-monomethyl ether 5000 and 0.2 M ammonium sulfate) and equilibrating against the precipitating solution at 19 °C. Crystallization drops also contained 0.1% octyl β-D-glucopyranoside and 0.4 mM acetoacetyl-CoA or 0.4 mM 4-nitrobutyryl-CoA.

Diffraction Data Collection. Data sets for GCD crystals obtained from solutions of acetoacetyl-CoA or 4-nitrobutyryl-CoA were collected in the same manner. Each crystal was mounted in a glass capillary, and diffraction data were collected at 4 °C on an R-AXIS II image plate detector system with a Rigaku RU200 rotating anode generator equipped with an Osmic confocal optics system. Both forms of crystals were isomorphous to each other with a hexagonal space group ($a = b = 117.0$ Å, $c = 128.0$ Å) and contained one monomer per asymmetric unit, as judged from the Matthew's coefficient ($V_m = 2.81$ Å^3/Da). The crystals obtained from the solution containing acetoacetyl-CoA diffracted to 2.1 Å, and the ones obtained from the 4-nitrobutyryl-CoA containing solution diffracted to 2.6 Å resolution. Both data sets were obtained from one crystal each. The diffraction data were processed with Denzo/Scalepack (*22*), and the data collection statistics are given in Table 1.

Table 1: Data Collection and Refinement Statistics

	GCD	4-NB-CoA-GCD[a]
Data Collection		
T (°C)	4	4
measured refls	90825	32735
unique refls	28832	13794
resolution (Å)	2.10	2.60
last shell (Å)	2.18−2.10	2.64−2.60
R_{sym} (last shell)	0.067(0.25)	0.088(0.32)
completeness (%)	93.8(69.7)	83.9(61.0)
$<I/\sigma(I)>$	9.4	11.3
Refinement		
no. of protein residues	390	390
no. of bound ligand		1
no. of water molecules	128	77
$R_{crystal}$ (%)	19.8	18.3
R_{free} (%)	22.3	23.9
rms deviation from ideality		
bond length (Å)	0.005	0.006
bond angle (deg)	1.1	1.2
Temperature Factors		
protein (Å^2)/no. of atoms	25.2/3065	20.1/3065
water molecule (Å^2)/no. of atoms	26.0/128	27.9/77
4-NB-CoA (Å^2)/no. of atoms		49.1/56

[a] GCD complexed with 4-nitrobut-2-enoyl-CoA.

Structure Determination. The numbering of the residues reported here is for the mature human wild-type GCD without the 44 amino acid mitochondrial targeting sequence (*23*) (NCBI accession number Q92947). The structure of the protein crystallized in the presence of acetoacetyl-CoA was solved and found to contain no ligand; therefore, hereafter it is referred to as simply the uncomplexed (or unliganded) GCD structure. The structure was solved using the molecular replacement procedure (MOLREP) implemented in the program package CCP4 (*24*) and using the monomer structure of MCAD (PDB code 3MDD) as the probe (*3*). Most of the MCAD residues were replaced with amino acids corresponding to those of the GCD sequence. Residues were modeled as alanine in cases where the sizes of the MCAD side chains were smaller than the corresponding GCD residues.

The cross rotation/translation searches gave one distinct solution ($\alpha = 0.97°$, $\beta = 89.69°$, and $\gamma = 177.29°$; $T_x = 0.252$, $T_y = 0.449$, and $T_z = 0.242$) and confirmed the space group to be $P6_422$. The structure of GCD with 4-nitrobutyryl-CoA (4-NBCoA-GCD) was solved by the difference Fourier method, as it was isomorphous to the crystals obtained in the presence of acetoacetyl-CoA. Both structures were refined using iterative cycles of CNS energy minimization (*25*), alternating with manual map-fitting and rebuilding on a Silicon Graphics workstation, using the TURBO-FRODO graphics software (*26*). Of the 394 residues of the monomer of mature human GCD, all but four residues (two at each

terminus) have been located in both structures. The final R_{cryst} and R_{free} values of the GCD structure were 19.9 and 22.3%, respectively; the corresponding values for 4-NB-CoA-GCD were 18.3 and 23.9%. Ramachandran plot analyses of both structures indicate that 90% of the residues reside in the most favored regions, and none are observed in disallowed regions. The refinement statistics for both structure determinations are listed in Table 1.

RESULTS AND DISCUSSION

Description of the Overall Polypeptide Fold of GCD. The overall structure of GCD is similar to that of other ACDs whose three-dimensional structures have been determined, including pig MCAD (*3*), a bacterial SCAD (*4*), human MCAD (*27*), human IVD (*5*), rat SCAD (*6*), and human isobutyryl-CoA dehydrogenase (IBD) (*7*). The rms deviations between the Cα atoms of GCD and other ACD structures, excluding loop regions with deletions and insertions, range from 1.1 Å with IVD (for 348 Cα atoms) to 1.4 Å with MCAD (for 347 Cα atoms). In the crystal structure of GCD, residues Glu3−Ala392 are easily identified; however, four residues, two each at the amino- and carboxyl-terminal regions, remain disordered. The overall structure of 4-NB-CoA-GCD is essentially the same as that of the unliganded structure, and the rms deviation between the Cα atoms of the two structures is only 0.2 Å.

The overall polypeptide fold of the GCD monomer consists of three domains: an α-helical bundle amino-terminal domain (helices A−F), a β-sheet domain in the middle (β-strands 1−7), and another α-helical domain at the carboxyl terminus (helices G−K) (Figure 1A). The FAD is located at the junction between the middle β-strand and the carboxyl-terminal α-helix domain of one subunit and the carboxyl-terminal domain of the neighboring subunit. The tetrameric molecule exhibits tetrahedral symmetry and can be viewed as a dimer of dimers. A ribbon diagram of a monomer and a tetramer of GCD is shown in Figure 1, and a section of the tetramer interface is shown in Figure 3. While the overall fold of the GCD structure is similar to other known ACD structures, there are several distinct features in the GCD structure. The most notable differences lie in the carboxyl- and amino-terminal regions of the monomer and in the loop between β-strands 4 and 5. This loop in GCD has only four residues, while the other ACDs have much larger number of residues, nine residues in both rat and bacterial SCADs and 12 residues in MCAD (Figure 2). The amino terminus of GCD is relatively well-ordered with only the first two residues being disordered, whereas Gly11 is the first residue that can be identified in the MCAD structure. The other ACDs have shorter amino-terminal extensions. A structure-based sequence alignment of all five ACD structures is shown in Figure 2. Differences in the carboxyl terminal domain of GCD are described next, as mutations in this region are found in patients with glutaric acidemia I (*28*).

Subunit Interactions and Mutations in the Carboxyl-Terminal Helix K and Its Extension. GCD has the longest extension at the carboxyl terminus following helix K among the ACDs (Figure 3). It also has the longest well-defined N-terminus, which makes van der Waals interactions with helix K interact with a neighboring subunit, resulting in more extensive intersubunit interfaces as compared to other ACDs.

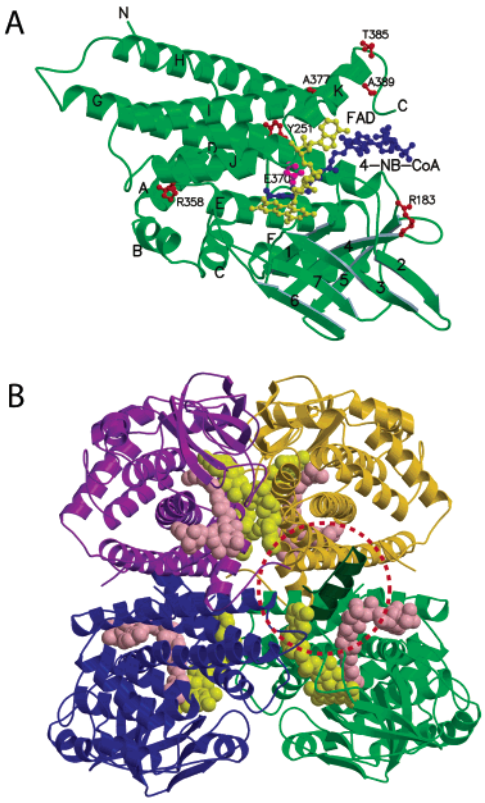

FIGURE 1: Overall polypeptide fold of GCD. Ribbon diagram of a monomer (A) and a tetramer (B) of GCD. Gold and purple subunits form one dimer, and green and blue subunits make the other dimer of the tetramer. Red dotted circle surrounding the dark green helix (helix K) of the green subunit depicts the subunit interface shown in Figure 3. Except Figures 2 and 4, all figures were generated using Molscript (*72*) and Raster3D (*73*)

Figure 3 shows the intersubunit interactions in the vicinity of the carboxyl terminus. In the tetrameric molecule of GCD, 30% of each monomer's surface is buried by the other three monomers, whereas only 24, 25, 26, and 27% of the monomer surface is buried in the IBD, IVD, SCAD, and MCAD structures, respectively. In GCD, helix K, with its longer extension loop, makes additional intersubunit interactions and plays a crucial role in the formation of the tetramer (Figure 3).

Mutations in the carboxyl-terminal region of GCD have been identified in patients with glutaric acidemia type 1. These mutations include Ala389Val, Ala389Glu, Thr385Met, Ala377Val, and Ala377Thr (Figure 3) (*28*). As expected, most of these mutant proteins dissociate to inactive monomers and/or dimers, indicating that these residues are important in tetramer formation. It should be noted that all of these substitutions increase the steric volume of the side chain. Ala389 lies at the extreme carboxyl-terminal loop of the monomer (Figures 1 and 3), and its main-chain carbonyl oxygen is making a hydrogen bond with Gln286. The side chain of Ala389 is in close contact with the N-terminal side of helix H (3.5−4.0 Å from the side chains of Arg284 and Gln289) (note that Gln289Glu is a pathogenic mutation) (*29*) of the neighboring subunit of the other dimer (gold subunit in Figures 1B and 3). Mutation of Ala389 to a bulky methionine or a charged bulky residue, glutamate, would result in severe steric hindrance, unless there were major conformational changes in the quaternary structure of the GCD tetramer. Thr385 is situated at the C-terminal end of

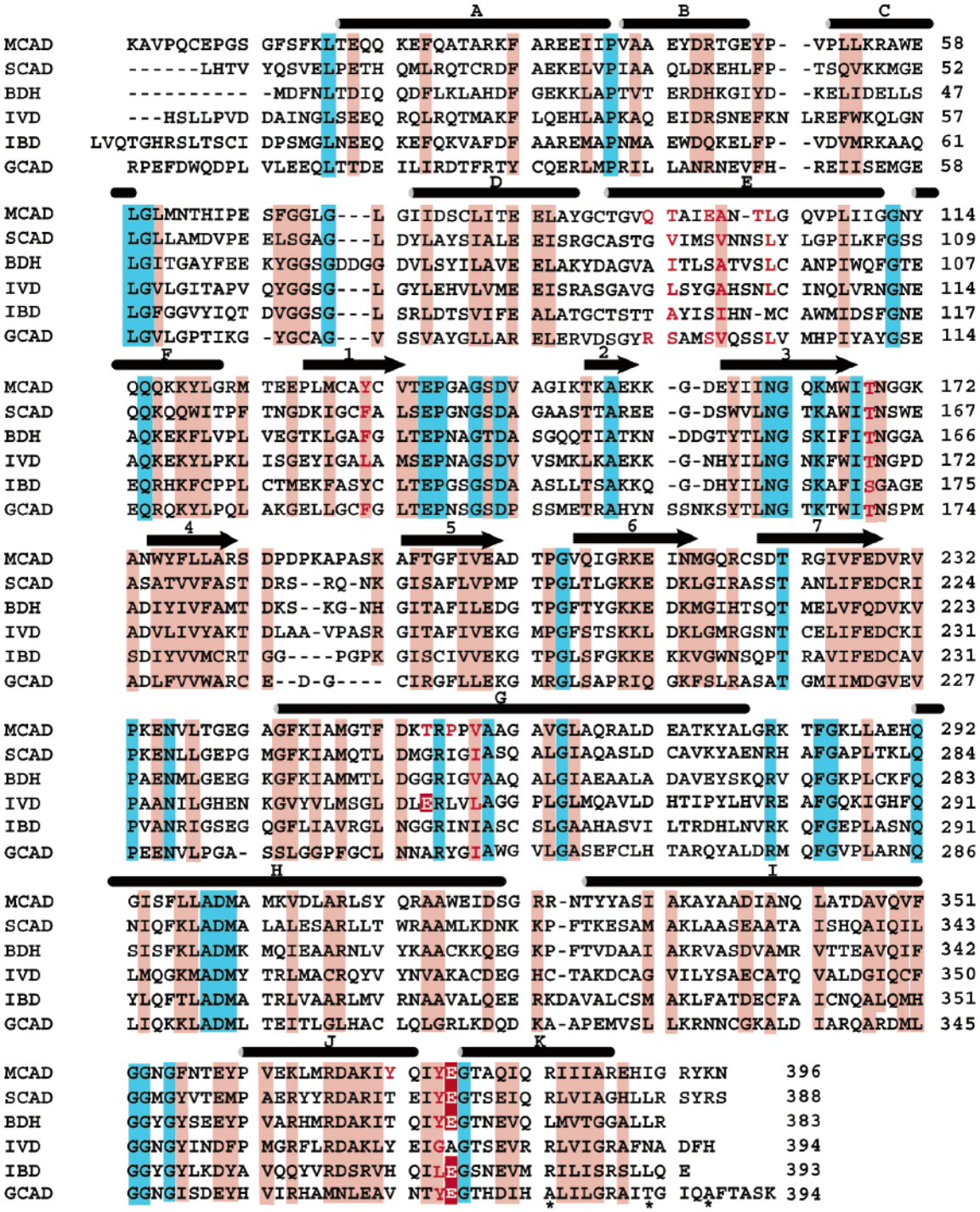

FIGURE 2: Structure-based sequence alignment of six acyl-CoA dehydrogenases. Identical residues are colored blue, and conserved residues are in pink. α-Helices are indicated with cylinders and are lettered; *β*-strands are shown with arrows and are numbered sequentially from N- to C-termini. Residues in red letters are those lining the binding cavity for the acyl moiety of thiolester substrates. Catalytic base in each ACD is shown with white letter with red background. Pathogenic mutation sites at the C-terminus of GCD are marked with an asterisk.

helix K (Figure 3) and makes van der Waals contacts with the side chains of Leu292 and Ala283 of the neighboring subunit. The side chain of Thr385 also makes an intersubunit hydrogen bond with the side chain of Gln289 and van der Waals contact with Leu292 (3.7 Å) of the neighboring subunit of the other dimer. Substitution of a bulky valine for Thr385 would interrupt these dimer−dimer interactions. Ala377 is located in the middle of helix K and makes close contacts (3.6∼4.5 Å) with Arg328 (helix I) of the same [note that Arg328Lys is a pathogenic mutation (*30*)]. Ala377 also makes a close contact (4.4 Å) with Ala293 of a neighboring subunit (gold subunit in Figure 3) in the other dimer and with Lys290 (4.5 Å) of another subunit (gold subunit in Figures 1B and 3). The dimer−dimer interaction here is that of helix−helix. Again, replacement of Ala377 with a relatively bulkier valine in a relatively hydrophilic environment would interrupt the overall folding and the tetramerization. The relative stability of Ala377Thr as compared to Ala377Val (*28*) is probably due to the hydrophilic nature of the threonine residue as compared to the valine substitution in relatively hydrophilic environment surrounded by Arg328, Lys290, and Asp374. In summary, mutations in this region

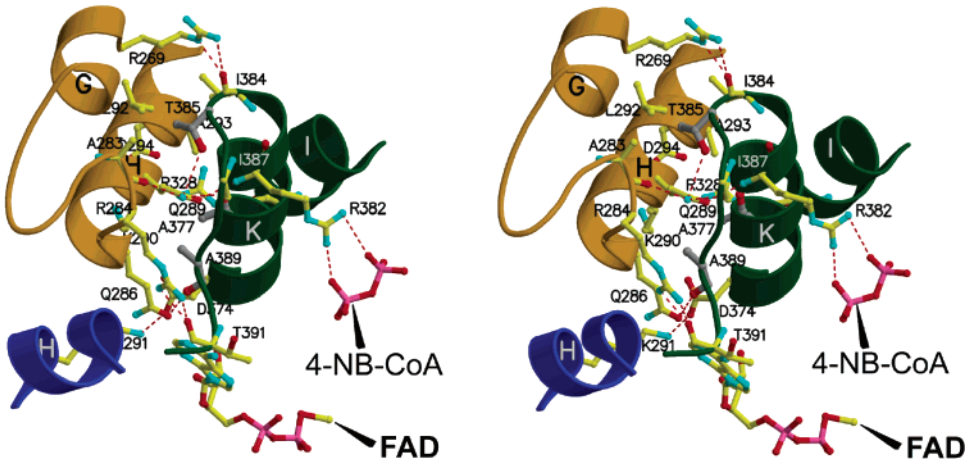

FIGURE 3: Subunit interactions involving the extreme carboxyl-terminal residues located in helix K of GCD (red circled region in Figure 1B). Color scheme for each subunit in the tetrameric interface is the same as in Figure 1B. Green and blue subunits form a dimer, and the gold subunit is from the other dimer of the tetramer. The adenosine-pyrophosphate moiety of FAD is shown at the bottom, and the pyrophosphate group of 4-NB-CoA, which makes salt bridges with Arg382, is shown on the lower right side of the figure.

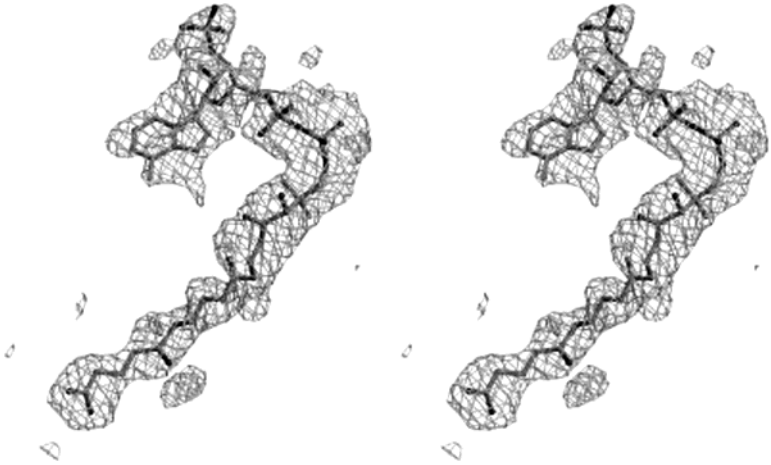

FIGURE 4: Stereo diagram of a model of 4-nitrobut-2-enoyl-CoA fitted into the electron density map. An omit $F_o - F_c$ difference Fourier map was contoured at 2.5σ level.

of the GCD molecule are generally detrimental to tetramer formation and weaken flavin and substrate binding (Figure 3).

A systematic mutation study on the C-terminus of IVD showed that deletion of a single residue at the C-terminus did not affect enzyme activity; however, a five-residue deletion mutant resulted in no detectable activity (*31*). No pathogenic mutations have been identified in the carboxyl-terminal region of MCAD or SCAD. The type III mutation identified in IVD is a frame-shift mutation resulting in an altered protein with misincorporation of eight residues at the C-terminus and 21 residues shorter than the wild type (*31*). This IVD mutant is not capable of forming a stable tetramer, indicating the importance of the C-terminal helix K in the tetramer formation.

GCD has five more residues at the C-terminus as compared to IVD, and Ala389 of GCD corresponds to the last residue in the IVD structure (Figure 2). Therefore, the GCD structure directly demonstrates that the C-terminus of GCD is more involved in the folding/stability of the tetrameric molecule than the other ACDs. In addition, as in the case of IVD and to a lesser extent in MCAD, Arg382 in GCD is located at the C-terminal end of helix K making salt bridges with the pyrophosphate linkages of 4-NBCoA (Figure 3). Thus, any significant structural disturbance at the C-terminal region of GCD might also affect substrate binding, leading to an inactive or inefficient enzyme.

Substrate-Binding Site. Although GCD crystals were obtained from a solution containing 0.4 mM acetoacetyl-CoA, no bound ligand was found in the structure. Instead, the substrate-binding pocket where the acyl chain of the thiolester would bind is filled with a string of three water molecules held by hydrogen bonds in a manner similar to that seen in the MCAD structure (*3*). One end of the string is fixed by three hydrogen bonds with the 2′-OH of the ribityl side chain of FAD and with both the amide nitrogen and a carboxyl oxygen of Glu370. These water molecules are displaced when the substrate binds to the enzyme. The difference Fourier map of the 4-nitrobutyryl-GCD structure yielded well-defined tubular densities extending to the *re* face of the FAD ring that could be easily fitted with a model of either 4-nitrobutyryl-CoA or 4-nitrobut-2-enoyl-CoA molecule (Figure 4). Since 4-nitrobutyryl-CoA is a substrate that can be oxidized by GCD functioning as an oxidase (*19*), a model of 4-nitrobut-2-enoyl-CoA, the product of the oxidation reaction, was used for the subsequent refinement of the 4-nitrobutyryl-GCD structure (hereafter, both the substrate, 4-nitrobutyryl-CoA, and the product, 4-nitrobut-2-enoyl-CoA,

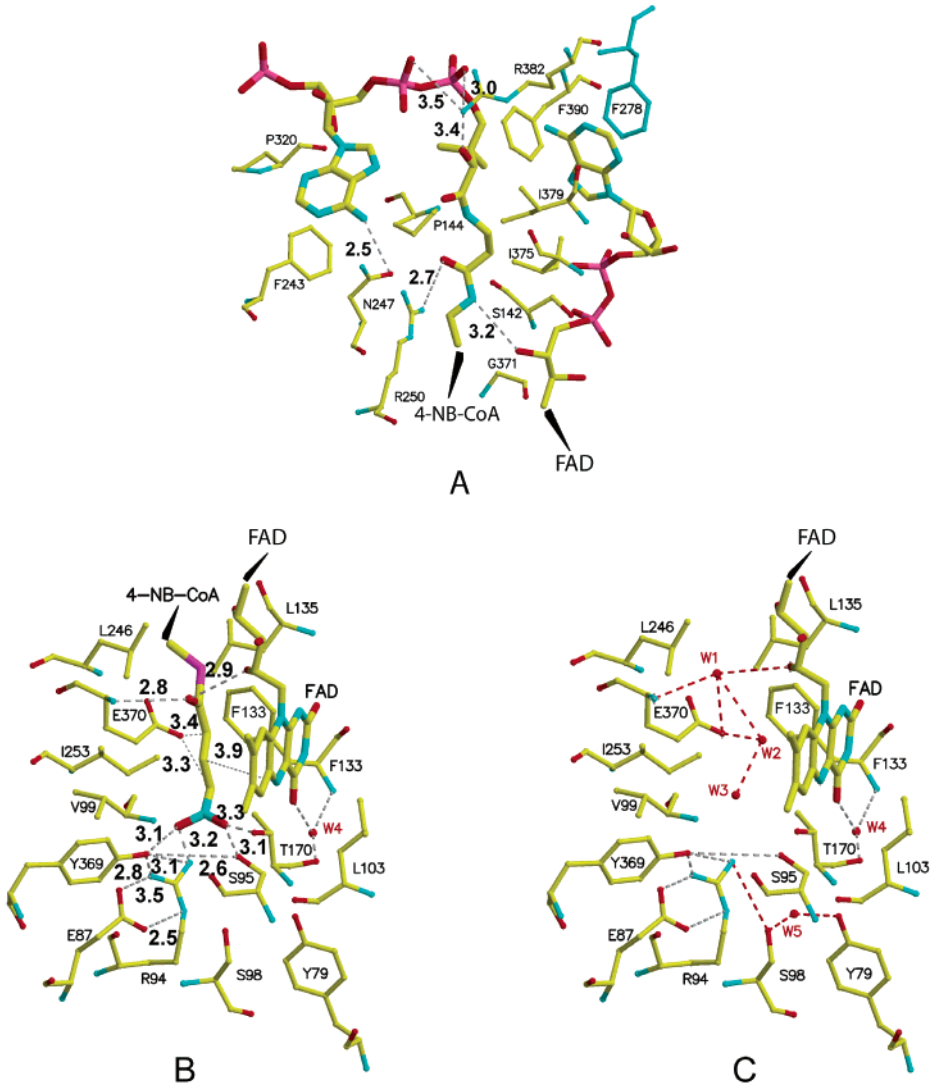

FIGURE 5: Flattened view of residues involved in binding 4-nitrobut-2-enoyl-CoA. Color scheme for atoms is carbon, yellow; nitrogen, blue; oxygen, red; phosphorus, magenta; and sulfur, pink. Potential hydrogen bonds observed only in the uncomplexed structure are indicated with red dashed lines, and those observed either in the complexed or in both structures are marked with gray dashed lines. (A) Residues surrounding the adenosine-pantetheine portion of CoA. Phe278 from the neighboring subunit is shown in blue. (B) Residues near the acyl-CoA thiolester moiety of the bound ligand in the structure of the complex. Distances between the catalytic base Glu370 to the C2 (3.4 Å) and C4 atoms (3.3 Å) of the substrate (for 1,3-prototropic shift) and between the N(5) of flavin and C3 of the substrate (3.9 Å, for hydride transfer) are indicated with black dotted lines. (C) Acyl-CoA binding cavity in the uncomplexed structure. Conformations of the residues making the active site cavity are virtually the same in complexed and uncomplexed structures. A string of three water molecules occupies the acyl thiolester cavity in the uncomplexed structure. Water molecules, W1, W2, W3, and W5, are observed only in the uncomplexed structure, whereas W4 is found in both structures and is common in all known ACD structures. For clarity, hydrogen-bonding distances involving water molecules are not shown.

are referred to as 4-NB-CoA). It is interesting to note that acetoacetyl-CoA, which binds to GCD with a submicromolar K_d (*18*), is not bound in the structure of crystals obtained in the presence of 0.4 mM concentration of the ligand. On the other hand, complexes are observed under the same condition with nitrobutyryl-CoA, which shows a weaker affinity to GCD (K_m = 14 μM (*19*)). Also, the complex of rat short-chain acyl-CoA dehydrogenase with acetoacetyl-CoA was crystallized under a similar condition but even at a higher pH (7.0) than GCD was (pH 6.5) (*6*). It is not known whether GCD promotes the hydrolysis of acetoacetyl-CoA in solution.

The only well-ordered water molecule near the active site of the structure of GCD complexed with 4-NB-CoA is a conserved water molecule found in all other ACD structures (*3*−*7*). This water is situated on the plane of isoalloxazine ring and is hydrogen bonded to the O4 atom of the ring (2.6 Å), main-chain carbonyl of Thr170 (2.8 Å), and the amide nitrogen of Phe133 (2.7 Å) (Figure 5B,C). This water molecule is about 6.1 Å away from the C4 atom of the bound ligand. There is no other well-ordered water molecule or large enough room for a water molecule in the vicinity of 4-NB-CoA. However, it has been shown that water can occupy the active site in the presence of the reaction intermediate, glutaconyl-CoA, since wild-type GCD exhibits significant enoyl-CoA hydratase activity with glutaconyl-CoA (*17*).

As with other known ACD structures, the adenosine diphosphate moiety of 4-NB-CoA is exposed to the solvent, whereas the pantetheine-fatty acyl portion of the ligand is deeply buried inside of the monomer structure (Figures 1 and 5). The residues lining the CoA moiety of the bound ligand in the GCD structure include (from the β-mercapto-

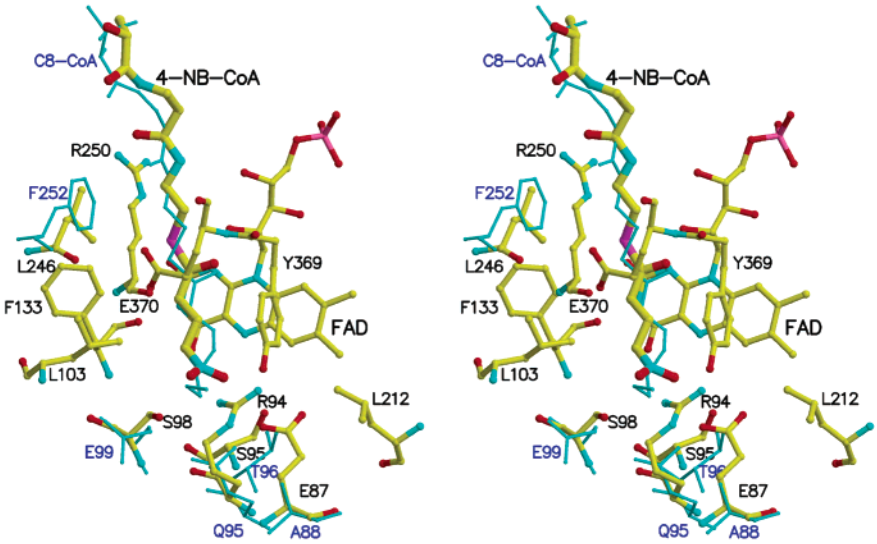

FIGURE 6: Stereo diagram of an overlay of the residues lining the acyl moiety of the substrate binding pockets of GCD and MCAD. Residues of GCD and 4-nitrobut-2-enoyl-CoA (thicker sticks) are shown in atom color (carbon, yellow; nitrogen, blue; oxygen, red; sulfur, pink; and phosphorus, magenta). For clarity, only residues of MCAD that are different from GCD are shown with thin blue sticks. The catalytic residue, Glu370, and the flavin ring sandwich the C_2-C_3 bond of the substrate. The plane of the nitro group of the ligand is almost perpendicular both to the plane of the thiolester group [—S—(C═O)—C1—C2═C3—C4—] and to the plane of the guanidinium group of Arg94.

ethanolamine portion and toward adenosine moiety) Pro144, Phe243, Asn247, Arg250 [note that Arg250Trp is a pathogenic mutation (*32*)], Pro320, Ile375, Ile379, Arg382, and Phe390 from one subunit and Phe278 from the adjacent subunit (Figure 5A). These residues form the entrance to the narrow tubular portion of the substrate-binding cavity. Except for Phe390, which is located in the extreme carboxyl-terminal extension (a unique feature of the GCD structure), all other residues are either conserved or replaced with similar residues in other known ACD structures (Figure 2). This is not unexpected since the CoA moiety of the substrate is common in all ACDs. Residues in the binding site for the fatty-acyl moiety are shown in Figure 5B. The binding pocket is shallower than that of MCAD and is about the same size as in SCAD. This relatively smaller size of the cavity is certainly responsible for the chain-length specificity of GCD for alternate substrates. In a survey of alternate substrates, the value of k_{cat}/K_m at pH 8 varies as glutaryl-CoA ≫ glutaramyl-CoA = monomethyl glutaryl-CoA > pentanoyl-CoA > hexanoyl-CoA > 5-hexenoyl-CoA ≫ 4-nitrobutyryl-CoA (*19*). The turnover number for butyryl-CoA (at 400 μM substrate concentration) is 0.11/s, which is only 1% of that for hexanoyl-CoA at similar conditions, indicating that the optimum acyl chain length is C5 ∼ C6.

Catalytic Base, Glutamate 370, of Human GCD. The C2−C3 bond of 4-NB-CoA is sandwiched between the carboxylate of Glu370 and the isoalloxazine ring of FAD, as seen in other ACD structures. The distance between C2 of the bound acyl-CoA and the carboxylate oxygen of Glu370 is 3.4 Å (Figure 5B), ideally positioned to abstract the *pro-R* α-proton on C2 to initiate the catalytic pathway. Glu370 was suggested to be the catalytic base based on sequence alignment with other acyl-CoA dehydrogenases, site-directed mutagenesis (*18*), and inactivation studies with 2-pentynoyl-CoA, which covalently modifies Glu370 (*33*). [Note that Glu370Lys is a pathogenic mutation (*34*).] The distance between the C3 atom of the substrate and the N(5) of the isoalloxazine ring of FAD is 3.9 Å, similar to that of MCAD (3.3 Å) (Figure 6) and suitable for hydride transfer of the *pro-R* hydrogen between the two atoms (*3*, *35*). Therefore, the structure is consistent with the initial steps in the reaction, deprotonation at C2 and hydride transfer from C3 to N(5), being the same as those catalyzed by MCAD. The carboxylate oxygen of Glu370 is also 3.3 Å away from the C4 atom, suggesting that Glu370 can access the C4 position of crotonyl-CoA (Figure 5B). Gomes and co-workers suggested, from their studies with *Pseudomonas fluorescens* GCD, that the conjugate acid of the catalytic base also protonates the transient crotonyl-CoA anion by a 1,3-prototropic shift following decarboxylation (*13*). Because human GCD and the *Pseudomonas* GCDs exhibit 64% sequence identity and the active site residues Arg94, Ser95, Ser98, Val99, Leu103, Phe133, Leu212, Tyr369, and Glu370 are 100% conserved, the reaction mechanism of the two GCDs, including the proposed 1,3-prototropic shift, are almost certainly identical.

GCD is rapidly inactivated by 2-pentynoyl-CoA by catalyzing a 1,3-prototropic shift (*33*). MCAD and SCAD are similarly inactivated by 2-alkynoyl-CoAs but more slowly than the inactivation of GCD (*36*−*39*). It is proposed that GCD is more rapidly inactivated because the active site is designed for the catalytic base to access the C4 position in the turnover (*33*). The distance between the carboxylate oxygen and the C4 atom of the 4-nitrobutyryl-CoA in GCD (3.3 Å) is considerably shorter than the corresponding distance of SCAD (3.5 Å), MCAD (4.9 Å), or IVD (6.3 Å). The rate of inactivation by 2-pentynoyl-CoA follows the order GCD ≫ SCAD > MCAD ≫ IVD. Thus, the rate of inactivation by the inhibitor is inversely related to the distance between the reacting atoms. The distance in the IVD structure was estimated from a modeled isovaleryl-CoA in the active site of the IVD structure in complex with CoA persulfide. The insensitivity of IVD toward the inhibitor is most likely due to a combination of a longer distance between the two atoms and the direction from which Glu255 approaches the C4 atom. An analogous situation has been observed with the double mutant of MCAD, Glu376Gly/

Thr255Glu, in which the catalytic base Glu376 was replaced with Thr255. This double mutant is not sensitive to irreversible inactivation by 2-octynoyl-CoA, consistent with the fact that the C4 atom is not readily accessible to the carboxylate of Glu255 as to that of Glu376 (*39*). On the other hand, the double mutant of IVD, Glu254Gly/Ala375Glu (a reverse mutant of the MCAD double mutant), is much more sensitive to inhibition by 2-pentynoyl-CoA than wild-type IVD (*38*).

The carbonyl oxygen of the thioester ligand in the GCD structure makes hydrogen bonds to the 2′-hydroxyl of the ribityl side chain of FAD (2.9 Å) and the amide nitrogen of Glu370 (2.8 Å). These hydrogen bonding interactions are observed in all other known ACD structures including MCAD, SCAD, IVD, and IBD (*7*, *9*). These interactions are crucial for the proper alignment of the substrate for C2 proton abstraction by Glu370 and contribute to the acidification of the C2 proton, which facilitates abstraction by general base catalysis (*35*). Thus, the structure of GCD is consistent with the proposal that Glu370 is the catalytic base that abstracts the C2 proton and is in position to reprotonate the C4 atom of the transient crotonyl-CoA anion. Glu370, together with the 2′-hydroxyl of the FAD ribityl chain, also contributes to the proper orientation of the substrate and acidification of the C2 proton to facilitate its deprotonation.

Role of Arginine 94 in Human GCD. Superposition of the active sites of GCD and MCAD are shown in Figure 6. Most of the residues lining the binding site are either identical or similar in the two structures, except for three notable differences: (a) a positively charged residue, Arg94, in GCD replaces the neutral residue, Gln95, in MCAD; (b) Ser98 in GCD substitutes for the negatively charged residue, Glu99, in MCAD; and (c) negatively charged Glu87 in GCD substitutes for apolar Ala88 in MCAD. Arg94 in GCD is unique; all other known ACD sequences have a neutral or polar residue at the corresponding position (Figure 2). It is proposed that Arg94 has several functions: (a) binding of the substrate, (b) orientation of the γ-carboxyl group for optimum decarboxylation, and (c) stabilization of the developing negative charge on C4, in the decarboxylation transition state and of the transient crotonyl-CoA anion. [Note that Arg94Gly and Arg94Lys are pathogenic mutations (*29*, *40*).] On the basis of the current structural studies and previous kinetic studies, Arg94 is involved in substrate binding and guiding of the γ-carboxylate into the binding site. The contribution of the Arg94/γ-carboxylate interaction to the total binding energy of glutaryl-CoA to the enzyme is significant but not essential. Replacement of Arg94 by glutamine, the corresponding residue in MCAD that is sterically similar to arginine, or by glycine, a pathogenic mutation, reduced k_{cat} to 2−3% that of the wild type and increased the K_m for glutaryl-CoA 10−16-fold. The K_m of the wild-type GCD for hexanoyl-CoA, which lacks the γ-carboxyl group, is almost the same as the K_m of Arg94Gly for glutaryl-CoA, consistent with the modest contribution of the Arg−carboxylate interaction to the total substrate-binding energy. The majority of the substrate-binding energy comes from the CoA moiety of the substrate that is not directly involved in any of the chemical steps, as seen with 3-oxoacid CoA-transferase (*41*). It has been shown that 3′-phosphate group of CoA moiety contributes 5.2 kJ/mol in the binding free energy with human MCAD (*42*). Also, the K_m of glutaryl-patetheine is some 590-fold higher than glutaryl-CoA reflecting the contribution of the 3′-phospho-5′ADP moiety of the CoA thiolester substrate in the binding process (*13*). In contrast, the substrate specificity of ACDs is conferred by the active site and the acyl-moiety of the substrate (*9*).

Arg94 may also be involved in the stabilization of developing negative charge at C4 in the decarboxylation transition state and the transient crotonyl-CoA anion. The distance between the guanidinium group of Arg94 and the C4 atom is 5.5 Å, close enough to stabilize the negative charge on the C4 atom of the crotonyl-CoA anion intermediate since Coulombic interactions are inversely proportional to the first power of the distance between the two charges. The next closest positively charged residue from the C4 atom is Arg250, located 9.7 Å away, which is conserved in all known ACD structures and interacts with oxygen on the pyrophosphate group of the CoA. Involvement of Arg94 in the electrostatic stabilization of transient anions is crucial (*18*).

Hydrogen-Bonding Network in the Active Site of Human GCD. As mentioned previously, the binding pocket for the fatty-acyl moiety of the substrate in the unliganded GCD structure is occupied by a string of three well-ordered water molecules. At the bottom of the binding site cavity exists a tightly woven hydrogen-bonding network involving Tyr369, Arg94, Glu87, and Ser95. Upon substrate binding, the water molecules are replaced with the fatty-acyl portion of the substrate; however, the conformations of residues surrounding the substrate remain almost the same as those in the unliganded structure (Figure 5B). The hydrogen-bonding network in the active site of GCD with 4-NB-CoA is even more striking. Figure 5B,C shows the vicinity of Arg94 in the 4-NB-CoA bound and unliganded structures, respectively, illustrating intricate interactions involving Arg94 and enzyme-bound 4-NB-CoA in the substrate-bound structure. Figure 6 shows a superposition of the residues involved in the acyl-CoA binding site of GCD and MCAD. The guanidinium group of Arg94 and the hydroxyl group of Tyr369 are within hydrogen-bonding distance of the terminal oxygen atoms of the 4-nitrobutyryl-CoA. The Nϵ of Arg94 forms a hydrogen bond with Glu87, which is also unique to GCD (Figures 2 and 6). Other ACDs have either a serine or an alanine at the corresponding position. The structure permits Tyr369 and Glu87 to orient Arg94 to interact with the γ-carboxylate oxygens of glutaryl-CoA.

Since 4-nitrobutyryl-CoA is isosteric and isoelectronic with the substrate, glutaryl-CoA, the binding of the γ-carboxyl group of the glutaryl-CoA should be identical to that of the nitro group of 4-NB-CoA observed in the current structure. Therefore, the constellation of residues surrounding the γ-carboxyl group of the glutaryl-CoA and the interactions among them can be assumed to be similar to the ones observed in the current structure. The orientation of the nitro group of the bound ligand, 4-NB-CoA (and presumably the γ-carboxyl group of glutaryl-CoA/ glutaconyl-CoA), with respect to the nearby residues (Arg94, Tyr369, Ser95, Glu87, and Thr170) is intriguing (Figures 5A and 6). The plane of the nitro group is almost orthogonal to the plane of the S−(C═O)−C2═C3−C4− in the acyl-CoA. Rotation about the C3−C4 bond of the γ-carboxyl plane in the structure is restricted to about 20° at most. This is due to the close proximity to the hydroxyl group of Tyr369 (3.1 Å), which

is also hydrogen bonded to Arg94 (3.2 Å) and Ser95 (3.1 Å). In addition, the guanidinium nitrogen atoms of Arg94 are hydrogen bonded to the carboxylic group of Glu87 (Figure 5B). The orthogonal arrangement of the γ-carboxylate group with respect to the plane of the polarized glutaconyl-CoA is the optimum orientation for decarboxylation, minimizing the stability of the conjugated double-bond system and facilitating C4−C5 bond breakage. Furthermore, the plane of the nitro group is almost perpendicular (~80°) to the plane of the guanidinium group of Arg94, again being in an optimal configuration for decarboxylation reaction (*43*). Therefore, it can be concluded that the hydrogen-bonding network involving Arg94, Tyr369, Ser98, Glu87, Thr170, and γ-carboxylate of glutaconyl-CoA is responsible for the optimum alignment of the γ-carboxylate group for decarboxylation. Hydrogen bonding of the guanidinium group of arginine with carboxylate group of ligand/substrate is frequently observed (*44*). Examples of these interactions supported by structural studies and investigation of site-directed mutants include prostaglandin synthase (*45*), deacetoxycephalosporin C synthase (*46*−*48*), 4-oxalocrotonate tautomerase (*49*), and carboxypeptidase (*50*). In all of these examples, arginine residues bind and orient a carboxylate substrate. Also, in the case of the tautomerase, one of the arginine residues (Arg39) binds substrate and serves as an electrostatic catalyst in enolization.

Mechanism of Decarboxylation by GCD. In the reductive half-reaction of the flavin of GCD the same structural features appear to participate as those found in other acyl-CoA dehydrogenases, allowing one to conclude that the mechanistic aspects of dehydrogenation are also similar. The substrate is polarized through the thiolester carbonyl by hydrogen bonding to the backbone amide of the catalytic base and the 2′-hydroxyl of the ribityl side chain of FAD (*3*, *9*). This reduces the pK_a of the *pro-R* proton at C2 for abstraction by Glu370 of GCD. Hydride is transferred to the *re* face of the flavin from C3 (*51*). The polarization of the system also contributes to increasing the potential of the dehydrogenase flavin to make reduction by the acyl-CoA favorable (*52*).

The decarboxylation of glutaconyl-CoA, the enzyme bound intermediate, is novel to GCD. Uncatalyzed decarboxylation of β,γ-unsaturated acids is a well-studied reaction. Decarboxylation of carboxylate ion occurs by an S_E1 mechanism in which the carbanion formed can be stabilized by an electron-withdrawing group (*53*−*56*). In general, the more stable the carbanion, the more favorable the decarboxylation (*57*).

There are several basic strategies known for enzymatic decarboxylation (*58*). In the case of mevalonate pyrophosphate decarboxylase, which involves a carbocation transition state, elimination of a negatively charged phosphate group follows decarboxylation (*59*). Many decarboxylases employ various schemes to delocalize negative charge following decarboxylation, and a stabilized carbanion intermediate is subsequently protonated. The latter may involve decarboxylation due to destabilization of the ground state such as in ornithine decarboxylase (*60*) and orotidine monophosphate decarboxylase (*61*). In ornithine decarboxylase, the anionic intermediate is stabilized by delocalization of electrons by the pyridoxal coenzyme. Stabilization by pyridoxal phosphate, thiamin, and divalent metals are well-known mechanisms for electron delocalization (*58*). An alternative to catalysis by pyridoxal or thiamine cofactors to achieve rate enhancement is stabilization of delocalized anionic transition state. This is the strategy employed by the catalytic antibody, 21D8 (*62*), malonyl-CoA decarboxylase (*63*), methyl malonyl-CoA decarboxylase (*64*), and the bacterial glutaconyl-CoA decarboxylase (*65*). In these decarboxylases, an anionic intermediate and the anionic transition state are stabilized by hydrogen bonding of the oxyanion of the thiolester carbonyl to the protein.

Hydrogen bonding of the carbonyl oxygen of substrate with backbone NH groups of His66 and Gly110 in *E. coli* methyl malonyl-CoA decarboxylase stabilizes the oxyanion resulting from decarboxylation (*64*). It is likely that the backbone NH of Glu370 and the 2′-hydroxyl in the ribityl side chain of FAD perform this function in GCD. In methyl malonyl-CoA decarboxylase, Tyr140 orients the carboxylate of the substrate orthogonal to the plane of the thiolester to facilitate decarboxylation by hydrogen bonding with the carboxylate. In GCD, it is likely that Tyr369 and Arg94, both of which form hydrogen bonds with γ-carboxylate of glutaconyl-CoA, function similarly. Several other enzymes that use acyl-CoA substrates such as β-ketoacyl synthase (*66*), thiolase (*67*), myristoyl-CoA:protein *N*-myristoyltransferase (*68*), and chalcone synthase (*63*), besides enzymes belonging to the crotonase superfamily (*69*), stabilize oxyanions that result from polarization of thiolester carbonyls. The example of the decarboxylating abzyme is pertinent because it demonstrates the effects of an active-site dipole in an otherwise relatively nonpolar environment and electrostatic stabilization of an anionic transition state by one or more arginine residues to achieve rate enhancement (*62*, *70*, *71*). The polar, aprotic active site of the enzyme is significant because studies of the noncatalyzed reaction show that hydrogen bonding of the carboxylate reduces the rate of decarboxylation (*63*). Thus, desolvation of the active site or decreased strength of hydrogen bonding of the carboxylate to a cationic amino acid side chain will contribute to rate enhancement.

In GCD, decarboxylation is initiated by polarization of the 2-enoyl-CoA via the thiolester carbonyl oxygen, which is evident in the three-dimensional structure with bound 4-nitrobutyryl-CoA. The extensive delocalization and electrostatic stabilization of the anionic transition state may be sufficient to provide the rate enhancement necessary to overcome unfavorable hydrogen bonding of the γ-carboxylate of glutaconyl-CoA to Arg94. It is perhaps significant that there is a monodentate, rather than a bidentate, hydrogen bond between the guanidinium of Arg94 and the γ-carboxylate, which would facilitate decarboxylation. The same oxygen is also hydrogen bonded to the phenolic hydrogen of Tyr369. The second oxygen of the γ-carboxylate is hydrogen bonded to the hydroxy group of Ser95 (which, in turn, is also hydrogen bonded to Tyr369) and the hydroxyl of Thr170. Protonation of the crotonyl-CoA anion may be accomplished by a 1,3-prototropic shift catalyzed by the conjugate acid of Glu370. The structure of the liganded GCD clearly shows that the 1,3-prototropic shift, originally proposed by Abeles and co-workers (*13*), is feasible because the oxygen of Glu370 is 3.3 Å from C4, which is optimal for such a shift.

In conclusion, the structures of GCD with and without an alternate substrate, 4-nitrobutyryl-CoA, reveal the roles of amino acid residues that are responsible for α,β-dehydrogenation and decarboxylation reactions, thus enabling us to describe the catalytic mechanism of this unique acyl-CoA dehydrogenase. The dehydrogenation reaction is in common with other acyl-CoA dehydrogenases. As observed in other acyl-CoA dehydrogenases, Glu370 is the catalytic base that abstracts the C2 proton, and the C3 hydrogen is transferred as a hydride ion to the N(5) atom of the isoalloxazine ring of FAD. The decarboxylation reaction, which is unique to GCD among the ACD family members, proceeds a via 1,3-prototropic shift catalyzed by the catalytic base Glu370 and is facilitated by a hydrogen-bonding network including Arg94, Glu87, Tyr369, Ser95, and Thr170. Further biochemical studies including site-specific mutagenesis are required to confirm the precise roles of these residues.

REFERENCES

1. Beinert, H. (2003) Acyl-Coenzyme A Dehydrogenases, in *The Enzymes*, 2nd ed. (Boyer, P. D., Lardy, H., and Myrback, K., Eds.) Vol. 7, pp 447−466, Academic Press, New York.
2. Lenich, A. C., and Goodman, S. I. (1986) The purification and characterization of glutaryl-coenzyme A dehydrogenase from porcine and human liver, *J. Biol. Chem. 261*, 4090−4096.
3. Kim, J. J. P., Wang, M., and Paschke, R. (1993) Crystal structures of medium-chain acyl-CoA dehydrogenase from pig liver mitochondria with and without substrate, *Proc. Natl. Acad. Sci. U.S.A. 90*, 7523−7527.
4. Djordjevic, S., Pace, C. P., Stankovich, M. T., and Kim, J. J. P. (1995) Three-dimensional structure of butyryl-CoA dehydrogenase from Megasphaera elsdenii, *Biochemistry 34*, 2163−2171.
5. Tiffany, K. A., Roberts, D. L., Wang, M., Paschke, R., Mohsen, A. W., Vockley, J., and Kim, J. J. P. (1997) Structure of human isovaleryl-CoA dehydrogenase at 2.6 Å resolution: structural basis for substrate specificity, *Biochemistry 36*, 8455−8464.
6. Battaile, K. P., Molin-Case, J., Paschke, R., Wang, M., Bennett, D., Vockley, J., and Kim, J. J. P. (2002) Crystal structure of rat short-chain acyl-CoA dehydrogenase complexed with acetoacetyl-CoA: comparison with other acyl-CoA dehydrogenases, *J. Biol. Chem. 277*, 12200−12207.
7. Battaile, K. P., Nguyen, T. V., Vockley J., and Kim, J. J. P. (2004) Structure of isobutyryl-CoA dehydrogenase and enzyme−product complex: Comparison with isovaleryl- and short-chain acyl-CoA dehydrogenases, *J. Biol. Chem. 279*, 16526−16534.
8. Ghisla, S., and Thorpe, C. (2004) Acyl-CoA dehydrogenases: A mechanistic overview, *Eur. J. Biochem. 271*, 494−508.
9. Kim, J.-J. P., and Miura, R. (2004) Acyl-CoA dehydrogenases and acyl-CoA oxidases: Structural basis for mechanistic similarities and differences, *Eur. J. Biochem. 271*, 483−493.
10. Telford, E. A., Moynihan, L. M., Markham, A. F., and Lench, N. J. (1999) Isolation and characterisation of a cDNA encoding the precursor for a novel member of the acyl-CoA dehydrogenase gene family, *Biochim. Biophys. Acta 1446*, 371−376.
11. Zhang, J., Zhang, W., Zou, D., Chen, G., Wan, T., Zhang, M., and Cao, X. (2002) Cloning and functional characterization of ACAD-9, a novel member of the human acyl-CoA dehydrogenase family, *Biochem. Biophys. Res. Commun. 297*, 1033−1042.
12. Djordjevic, S., Dong, Y., Paschke, R., Frerman, F. E., Strauss, A. W., and Kim, J. J. P. (1994) Identification of the catalytic base in long-chain acyl-CoA dehydrogenase, *Biochemistry 33*, 4258−4264.
13. Gomes, B., Fendrich, G., and Abeles, R. H. (1981) Mechanism of action of glutaryl-CoA and butyryl-CoA dehydrogenases. Purification of glutaryl-CoA dehydrogenase, *Biochemistry 20*, 1481−1490.
14. Ghisla, S., Thorpe, C., and Massey, V. (1984) Mechanistic studies with general acyl-CoA dehydrogenase and butyryl-CoA dehydrogenase: evidence for the transfer of the β-hydrogen to the flavin *N*(5)-position as a hydride, *Biochemistry 23*, 3154−3161.
15. Schopfer, L. M., Massey, V., Ghisla, S., and Thorpe, C. (1988) Oxidation−reduction of general acyl-CoA dehydrogenase by the butyryl-CoA/crotonyl-CoA couple. A new investigation of the rapid reaction kinetics, *Biochemistry 27*, 6599−6611.
16. Dwyer, T. M., Rao, K. S., Goodman, S. I., and Frerman, F. E. (2000) Proton abstraction reaction, steady-state kinetics, and oxidation−reduction potential of human glutaryl-CoA dehydrogenase, *Biochemistry 39*, 11488−11499.
17. Westover, J. B., Goodman, S. I., and Frerman, F. E. (2001) Binding, hydration, and decarboxylation of the reaction intermediate glutaconyl-coenzyme A by human glutaryl-CoA dehydrogenase, *Biochemistry 40*, 14106−14114.
18. Dwyer, T. M., Rao, K. S., Westover, J. B., Kim, J. J. P., and Frerman, F. E. (2001) The function of Arg-94 in the oxidation and decarboxylation of glutaryl-CoA by human glutaryl-CoA dehydrogenase, *J. Biol. Chem. 276*, 133−138.
19. Rao, K. S., Vander Velde, D., Dwyer, T. M., Goodman, S. I., and Frerman, F. E. (2002) Alternate substrates of human glutaryl-CoA dehydrogenase: structure and reactivity of substrates and identification of a novel 2-enoyl-CoA product, *Biochemistry 41*, 1274−1284.
20. Kim, J.-J. P., Wang, M., Paschke, R., Goodman, S. I., Biery, B., and Frerman, F. E. (1999) The crystal structure of human glutaryl-CoA dehydrogenase, in *Flavins and Flavoproteins* (Ghisla, S., Kroneck, P., Macheroux, P., and Sund, H., Eds.) pp 539−543, Agency for Scientific Publications, Berlin.
21. McPherson, A. (1999) *Crystallization of Biological Macromolecules*, Cold Spring Harbor Laboratory Press, Plainview, NY.
22. Otwinowski, Z., and Minor, W. (1996) *Processing of X-ray Diffraction Data Collected in Oscillation Mode* (Carter, C., and Sweet, R. M., Eds.) pp 307−325, Academic Press, Boston.
23. Goodman, S. I., Kratz, L. E., DiGiulio, K. A., Biery, B. J., Goodman, K. E., Isaya, G., and Frerman, F. E. (1995) Cloning of glutaryl-CoA dehydrogenase cDNA and expression of wild-type and mutant enzymes in *Escherichia coli*, *Hum. Mol. Genet. 4*, 1493−1498.
24. CCP4 (1994) The CCP4 Suite: Programs for Protein Crystallography, *Acta Crystallogr. D50*, 760−763.
25. Brunger, A. T., Adams, P. D., Clore, G. M., DeLano, W. L., Gros, P., Grosse, K., Jiang, J. S., Kuszewski, J., Nilges, M., Pannu, N. S., Read, R. J., Rice, L. M., Simonson, T., and Warren, G. L. (1998) Crystallography and NMR system: A new software suite for macromolecular structure determination, *Acta Crystallogr. D54*, 905−921.
26. Roussel, A., Inisan, A. G., Knoop-Mouthuy, A., and Cambillau, C. (1999) *Turbo-Frodo, Version OpenGL: 1*, Marseille, France, CNRS/Universitite, Marseille.
27. Lee, H. J., Wang, M., Paschke, R., Nandy, A., Ghisla, S., and Kim, J. J. P. (1996) Crystal structures of the wild-type and the Glu376Gly/Thr255Glu mutant of human medium-chain acyl-CoA dehydrogenase: influence of the location of the catalytic base on substrate specificity, *Biochemistry 35*, 12412−12420.
28. Westover, J. B., Goodman, S. I., and Frerman, F. E. (2003) Pathogenic mutations in the carboxyl-terminal domain of glutaryl-CoA dehydrogenase: effects on catalytic activity and the stability of the tetramer, *Mol. Genet. Metab. 79*, 245−256.
29. Goodman, S. I., Stein, D. E., Schlesinger, S., Christensen, E., Schwartz, M., Greenberg, C. R., and Elpeleg, O. N. (1998) Glutaryl-CoA dehydrogenase mutations in glutaric acidemia (type I): review and report of 30 novel mutations, *Hum. Mutat. 12*, 141−144.
30. Busquets, C., Merinero, B., Christensen, E., Gelpi, J. L., Campistol, J., Pineda, M., Fernandez-Alvarez, E., Prats, J. M., Sans, A., Arteaga, R., Marti, M., Campos, J., Martinez-Pardo, M., Martinez-Bermejo, A., Ruiz-Falco, M. L., Vaquerizo, J., Orozco, M., Ugarte, M., Coll, M. J., and Ribes, A. (2000) Glutaryl-CoA dehydrogenase deficiency in Spain: evidence of two groups of patients, genetically and biochemically distinct, *Pediatr. Res. 48*, 315−322.
31. Volchenboum, S. L., Mohsen, A. W., Kim, J. J. P., and Vockley, J. (2001) Arginine 387 of human isovaleryl-CoA dehydrogenase plays a crucial role in substrate/product binding, *Mol. Genet. Metabol. 74*, 226−237.
32. Schwartz, M., Christensen, E., Superti-Furga, A., and Brandt, N. J. (1998) The human glutaryl-CoA dehydrogenase gene: report of intronic sequences and of 13 novel mutations causing glutaric aciduria type I, *Hum. Genet. 102*, 452−458.
33. Rao, K. S., Albro, M., Vockley, J., and Frerman, F. E. (2003) Mechanism-based inactivation of human Glutaryl-CoA dehydrogenase by 2-Pentynoyl-CoA: Rationale for enhanced reactivity, *J. Biol. Chem. 278*, 26432−26350.

34. Biery, B. J., Stein, D. E., Morton, D. H., and Goodman, S. I. (1996) Gene structure and mutations of glutaryl-coenzyme A dehydrogenase: impaired association of enzyme subunits that is due to an A421V substitution causes glutaric acidemia type I in the Amish, *Am. J. Hum. Genet. 59*, 1006−1011.
35. Engst, S., Vock, P., Wang, M., Kim, J. J. P., and Ghisla, S. (1999) Mechanism of activation of acyl-CoA substrates by medium-chain acyl-CoA dehydrogenase: interaction of the thioester carbonyl with the flavin adenine dinucleotide ribityl side chain, *Biochemistry 38*, 257−267.
36. Powell, P. J., and Thorpe, C. (1988) 2-Octynoyl coenzyme A is a mechanism-based inhibitor of pig kidney medium-chain acyl coenzyme A dehydrogenase: isolation of the target peptide, *Biochemistry 27*, 8022−8028.
37. Lundberg, N. N., and Thorpe, C. (1993) Inactivation of short-chain acyl-coenzyme A dehydrogenase from pig liver by 2-pentynoyl-coenzyme A, *Arch. Biochem. Biophys. 305*, 454−459.
38. Schaller, R. A., Mohsen, A. W., Vockley, J., and Thorpe, C. (1997) Mechanism-based inhibitor discrimination in the acyl-CoA dehydrogenases, *Biochemistry 36*, 7761−7768.
39. Nandy, A., Kieweg, V., Krautle, F. G., Vock, P., Kuchler, B., Bross, P., Kim, J. J. P., Rasched, I., and Ghisla, S. (1996) Medium-long-chain chimeric human Acyl-CoA dehydrogenase: medium-chain enzyme with the active center base arrangement of long-chain Acyl-CoA dehydrogenase, *Biochemistry 35*, 12402−12411.
40. Zschocke, J., Quak, E., Gludberg, P., and Hoffmann, G. F. (2000) Mutation analysis in glutaric acidemia type I, *J. Med. Genet. 37*, 177−181.
41. Whitty, A., Fierke, C. A., and Jencks, W. P. (1995) Role of binding energy with coenzyme A in catalysis by 3-oxoacid coenzyme A transferase, *Biochemistry 34*, 11678−11689.
42. Peterson, K. L., and Srivastava, D. K. (1997) Functional role of a distal (3′-phosphate) group of CoA in the recombinant human liver medium-chain acyl-CoA dehydrogenase-catalyzed reaction, *Biochem. J. 325*, 751−760.
43. Singh, J., Thornton, J. M., Snarey, M., and Campbell, S. F. (1987) The geometries of interacting arginine-carboxyls in proteins, *FEBS Lett. 224*, 161−171.
44. Riodan, J. F., McElvany, K. D., and Borders, C. L. (1977) Arginyl residues: anion recognition sites in enzymes, *Science 195*, 884−886.
45. Bhattacharyya, D. K., Lecomte, M., Rieke, C. J., Garavito, M., and Smith, W. L. (1996) Involvement of arginine 120, glutamate 524, and tyrosine 355 in the binding of arachidonate and 2-phenylpropionic acid inhibitors to the cyclooxygenase active site of ovine prostaglandin endoperoxide H synthase-1, *J. Biol. Chem. 271*, 2179−2184.
46. Lee, H. J., Dai, Y. F., Shiau, C. Y., Schofield, C. J., and Lloyd, M. D. (2003) The kinetic properties of various R258 mutants of deacetoxycephalosporin C synthase, *Eur. J. Biochem. 270*, 1301−1307.
47. Lee, H. J., Lloyd, M. D., Clifton, I. J., Harlos, K., Dubus, A., Baldwin, J. E., Frere, J. M., and Schofield, C. J. (2001) Alteration of the cosubstrate selectivity of deacetoxycephalosporin C synthase, The role of arginine 258, *J. Biol. Chem. 276*, 18290−18295.
48. Lipscomb, S. J., Lee, H. J., Mukherji, M., Baldwin, J. E., Schofield, C. J., and Lloyd, M. D. (2002) The role of arginine residues in substrate binding and catalysis by deacetoxycephalosporin C synthase, *Eur. J. Biochem. 269*, 2735−2739.
49. Czerwinski, R. M., Harris, T. K., Johnson, W. H. J., Legler, P. M., Stivers, J. T., Mildvan, A. S., and Whitman, C. P. (1999) Effects of mutations of the active site arginine residues in 4-oxalocrotonate tautomerase on the pK_a values of active site residues and on the pH dependence of catalysis, *Biochemistry 38*, 12358−12366.
50. Phillips, M. A., Fletterick, R., and Rutter, W. J. (1990) Arginine 127 stabilizes the transition state in carboxypeptidase, *J. Biol. Chem. 265*, 20692−20698.
51. Thorpe, C., and Kim, J. J. P. (1995) Structure and mechanism of action of the acyl-CoA dehydrogenases, *FASEB J. 9*, 718−725.
52. Pellett, J. D., Sabaj, K. M., Stephens, A. W., Bell, A. F., Wu, J., Tonge, P. J., and Stankovich, M. T. (2000) Medium-chain acyl-coenzyme A dehydrogenase bound to a product analogue, hexadienoyl-coenzyme A: effects on reduction potential, pK_a, and polarization, *Biochemistry 39*, 13982−13992.
53. Oae, S., Tagaki, W., Uneyama, K., and Minamida, I. (1968) 3d-orbital resonance in divalent sulfide-X: The effects of alpha-aryl and alpha-alkylmercapto groups on the rate of decarboxylation of alpha-substituted carboxylic acids, *Tetrahedron 24*, 5283−5291.
54. Buncel, E., Venkatachalam, T. K., and Menon, B. C. (1984) Carbanion mechanisms. Part 14. A spectrophotometric study of 4-nitro-, 2,4-dinitro-, and 2,4,6-trinitro carbanions. Decarboxylation of {nitrophenyl}acetate anions, *J. Org. Chem. 49*, 413−417.
55. Seruga, P., Bunnett, J. F., and Villanova, L. (1985) Substituent effects on the decarboxylation of dinitrobenzoate ions. Representative aromatic S_E1 reactions, *J. Org. Chem. 50*, 1041−1045.
56. Smith, M. B., and March, J. (2001) *March's Advanced Organic Chemistry- Reactions, Mechanisms, and Structure*, 5th ed., pp 675−849, John Wiley and Sons, New York.
57. March, J. (1963) The decarboxylation of organic acids. *J. Chem. Educ. 40*, 212−213.
58. Kosower, E. M. (1962) *Molecular Biochemistry*, pp 71−90, McGraw-Hill, New York.
59. Dhe-Paganon, S., Magrath, J., and Abeles, R. H. (1994) Mechanism of mevalonate pyrophosphate decarboxylase: evidence for a carbocationic transition state, *Biochemistry 33*, 13355−13362.
60. Jackson, L. K., Brooks, H. B., Myers, D. P., and Phillips, M. A. (2003) Ornithine decarboxylase promotes catalysis by binding the carboxylate in a buried pocket containing phenylalanine 397, *Biochemistry 42*, 2933−2940.
61. Wu, N., Mo, Y., Gao, J., and Pai, E. F. (2000) Electrostatic stress in catalysis: structure and mechanism of the enzyme orotidine monophosphate decarboxylase, *Proc. Natl. Acad. Sci. U.S.A. 97*, 2017−2022.
62. Hotta, K., Lange, H., Tantillo, D. J., Houk, K. N., Hilvert, D., and Wilson, I. A. (2000) Catalysis of decarboxylation by a preorganized heterogeneous microenvironment: crystal structures of abzyme 21D8, *J. Mol. Biol. 302*, 1213−1225.
63. Jez, J. M., Ferrer, J. L., Bowman, M. E., Dixon, R. A., and Noel, J. P. (2000) Dissection of malonyl-coenzyme A decarboxylation from polyketide formation in the reaction mechanism of a plant polyketide synthase, *Biochemistry 39*, 890−902.
64. Benning, M. M., Haller, T., Gerlt, J. A., and Holden, H. M. (2000) New reactions in the crotonase superfamily: structure of methylmalonyl CoA decarboxylase from *Escherichia coli*, *Biochemistry 39*, 4630−4639.
65. Buckel, W. (2001) Sodium ion-translocating decarboxylases, *Biochim. Biophys. Acta 1505*, 15−27.
66. Witkowski, A., Joshi, A. K., and Smith, S. (2002) Mechanism of the β-ketoacyl synthase reaction catalyzed by the animal fatty acid synthase, *Biochemistry 41*, 10877−10887.
67. Kursula, P., Ojala, J., Lambeir, A. M., and Wierenga, R. K. (2002) The catalytic cycle of biosynthetic thiolase: a conformational journey of an acetyl group through four binding modes and two oxyanion holes, *Biochemistry 41*, 15543−15556.
68. Farazi, T. A., Manchester, J. K., Waksman, G., and Gordon, J. I. (2001) Presteady-state kinetic studies of *Saccharomyces cerevisiae* myristoylCoA: protein *N*-myristoyltransferase mutants identify residues involved in catalysis, *Biochemistry 40*, 9177−9186.
69. Holden, H. M., Benning, M. M., Haller, T., and Gerlt, J. A. (2001) The crotonase superfamily: divergently related enzymes that catalyze different reactions involving acyl coenzyme a thioesters, *Acc. Chem. Res. 34*, 145−157.
70. Na, J., Houk, K. N., and Hilvert, D. (1996) Transition state of the base-promoted ring opening of isoxazoles: Theoretical prediction of catalytic functionalities and design of haptens for antibody production, *J. Am. Chem. Soc. 118*, 6462−6471.
71. Ujaque, G., Tantillo, D. J., Hu, Y., Houk, K. N., Hotta, K., and Hilvert, D. (2003) Catalysis on the coastline: theozyme, molecular dynamics, and free energy perturbation analysis of antibody 21D8 catalysis of the decarboxylation of 5-nitro-3-carboxybenzisoxazole, *J. Comput. Chem. 24*, 98−110.
72. Kraulis, P. J. (1991) MolScript: a program to produce both detailed and schematic plots of protein structures, *J. Appl. Crystallogr. 24*, 946−950.
73. Merritt, E. A., and Murphy, M. E. P. (1994) Raster3D, *Acta Crystallogr. D50*, 869−873.

BI049290C